Hindawi Publishing Corporation
International Journal of Differential Equations
Volume 2012, Article ID 376350, 21 pages
doi:10.1155/2012/376350

Research Article

Unsteady Integrodifferential Equation of Fluid-Structure Interaction in Constricted Collapsible Tube Model of Diseased Human Coronary Artery

Eric Velaski Tuema and Olusegun Ilegbusi

Department of Mechanical Engineering, University of Central Florida, Orlando, FL 32816, USA

Correspondence should be addressed to Olusegun Ilegbusi, ilegbusi@ucf.edu

Received 1 July 2011; Accepted 15 December 2011

Academic Editor: Mayer Humi

Unsteady flow in a collapsible tube is analyzed to simulate a diseased human coronary artery. The novelty of the approach is that the set of equations governing the fluid-structure interaction is reduced to a single integrodifferential equation in the transient state. The equation is then solved using the finite difference method to obtain the flow characteristics and compliant wall behavior. Three control parameters are investigated, namely, Reynolds number, inlet transmural pressure, and the wall thickness. The predicted wall deflection is quite large at low Reynolds numbers, suggesting possible approach to breakdown in equilibrium. The transmural pressure increases with wall deflection and bulges appear at the ends of the membrane indicating critical stage of stability, consistent with previous studies. Increase in wall thickness reduces the wall deflection and ultimately results in its collapse which may indicate another breakdown in equilibrium. An increase in internal pressure is required to maintain membrane stability.

1. Introduction

This paper describes a two-dimensional (2D) analytical study of collapsible tube simulating unsteady flow in a stenosed coronary artery. The effect is investigated of peristaltic flow in a geometrically nonlinear elastic tube, whose walls deform due to the transient transmural pressure. The arterial wall motion results in a strong fluid-structure interaction. The study is based on the hypothesis that the transient fluid-structure interaction in such a channel could be adequately represented as a single integrodifferential equation which can be solved using finite-difference numerical method. The novelty of the study is the analysis of unsteady flow and the methodology employed to solve the resulting integrodifferential equation.

The problem posed by fluid flow through flexible tubes with relatively thin walls is theoretically challenging and practically significant. The theoretical challenges are due to the interaction between the fluid flow and the elastic channel walls. Thus, fluid flow and structural parameters have to be computed simultaneously. In addition, the boundary conditions cannot be completely defined in advance, due to the continuously evolving boundary. The practical significance of these problems are considerable, in particular in bioengineering and biomedical systems because of their pivotal role in describing fluid flow in living organs including cardiovascular, respiratory, and urinary systems [1]. In particular, vessels experiencing compressive transmural pressure and consequent remodeling include the vein above the heart, the coronary arteries during systole, and the airways during forced expiration [2]. The early theoretical investigations [3, 4] despite reproducing flow characteristics were unable to predict the details of wall deformation. Most previous studies have also focused on steady flow situations in order to reduce the computational complexity. The present paper relaxes these simplifications by analyzing the unsteady flow of deformable tube and solving the resulting integrodifferntial equations.

Flows in collapsible tubes have been thoroughly reviewed in a previous study [5]. The approach used in solving such flows depends on the flow situation. Steady flow with low Reynolds number and negligible inertia is referred to as lubrication-type flow [6]. Unsteady flow in which variations in the flow direction are significant is called Stokes-type flow [6]. In this case, the Reynolds number is typically high and inertia is taken into consideration. The full Navier-Stokes equations must be solved in such a situation, requiring numerical analysis. The elastic channel wall is usually modeled as a membrane using the thin-shell theory with negligible bending stiffness.

Several methods of modeling flow in flexible tubes have been summarized in a recent study [1]. The study discusses the significance of the interaction between fluid flow within the tube and the wall deformation. The physiological implications of such fluid-structure interaction are also fully explored, including human cardiovascular and respiratory systems. The study concludes that despite the intense interest, the diverse mechanisms generating instabilities in single-phase flow through a flexible tube remain only partially understood. Therefore, there is a need for more systematic investigations that will shed light on generic relationships and experimental observations as well as physiological applications carefully accounting for the mechanical properties of tissues.

Modeling of flow in collapsible tubes has ranged from one-dimensional (1D) to 3D [7–17]. Shapiro [7] investigated 1D steady flow in a partially collapsed thin-walled tube and demonstrated that steady flow cannot exist in a collapsible tube under flow velocity as high as the speed of propagation of small amplitude pressure waves. Under these conditions, choking and unsteadiness set in. Two-dimensional studies [8–11] include zero Reynolds number steady flow or finite Reynolds number unsteady flow, in which part of the rigid wall was replaced by an elastic membrane. Pedley [12] investigated the breakdown steady flow using lubrication theory in a symmetric 2D channel. The resulting nonlinear ordinary differential equations were solved numerically. The results suggest that reducing the longitudinal tension in the channel wall increases the deformation for the same flow rate and external pressure. Djordjevic and Vukobratovic [13] studied of steady, viscous flow in a collapsible channel at both low and high Reynolds numbers. The elastic channel wall behavior was modeled by a geometrically nonlinear Karman shell theory. In each case, a single integrodifferential equation was derived to describe the wall configuration and the governing equation was numerically solved. The wall configuration was predicted as a function of some control parameters. Other studies considered steady deformations of the

fully three-dimensional system [14, 15]. The tube wall was modeled as a circular cylindrical shell and geometrically nonlinear shell theory was used to model its large nonaxisymmetric deformation (post buckling). The fluid flow was modeled using lubrication theory assuming low Reynolds numbers and a small wall slope in the direction of the flow. Pedley [16] investigated flow through collapsible arteries. More recently, perturbation and numerical methods were used to examine the drag reduction in gel-lined tubes and other surfaces [17].

Most of the variety of models applied to collapsible tube have used as the pivotal parameter, the transmural pressure, defined as the difference between the external and internal pressure. If this pressure differential is negative the channel experiences internal pressure, giving it a spherical cross-sectional shape [18]. If the pressure differential is positive the channel walls collapse. Many of the previous studies [7, 12, 16] have also focused on steady flow problems due to the complexity of the equations governing the fluid flow and wall configuration, and in order to reduce the number of control parameters. Other studies considering unsteady flow problems employed the Finite Element Method (FEM) to solve the governing equations [1, 10]. Application of FEM to the type of problem considered is complicated by the variety of competing factors including interpolations at the nodes of discretized elements, strain-displacement relation, stress-strain calculation, element equilibrium equations, global equilibrium equations, and so forth [19].

In the present study, unsteady 2D Stokes equations will be derived and used to analyze the fluid-structure interaction at relatively low Reynolds number. The governing equations reduce to a single integrodifferential equation which is solved numerically by the finite-difference method (FDM). The advantage of FDM is its recursive approach which allows convenient and accurate representation of the nonlinear fluid flow equations. The effect on flow and wall configurations are investigated of three control parameters, the Reynolds number (or equivalently, the inlet velocity), transmural pressure, and wall thickness.

2. Formulation

2.1. Hypothesis

The transient fluid-structure interaction in a collapsible tube model of diseased human coronary artery could be represented as a single integrodifferential equation which can be solved using finite-difference numerical method.

This section describes the derivation and solution of the governing equation. The transmural pressure distribution on the channel wall is determined from lubrication theory. The nonlinear Karman plate theory is used to express the wall elastic behavior. A single integrodifferential equation is derived for the first time, governing the membrane behavior in the transient state. The equations for pressure and compliant wall are solved using finite difference methods. This analytical approach differs from the relatively expensive application of finite-element method as in previous studies.

2.2. Geometry

Consider an idealized symmetrical diseased human coronary artery (Figures 1 and 2) through which an incompressible, viscous fluid is flowing. This two-dimensional (2D) model is inspired from Djordjevic and Vukobratovic's [13] where the flow is assumed to be fully developed at the entrance ($x^* = 0$) of the segment and remains laminar throughout. Thus

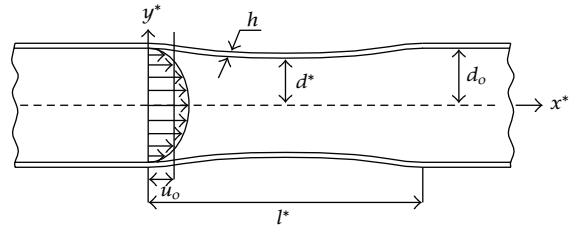

Figure 1: Schematic sketch of 2D collapsible channel.

the velocity profile in the segment is independent of Reynolds number. The artery wall configuration is driven by stresses acting on the surface. The elastic wall configuration is assumed to be a plate. Thus both wall inertia and fluid inertia are represented in the calculation.

We employ lubrication theory, assuming small wall slope and negligible wall inertia [12, 13]. The segment has length l^* comprising parallel compliant walls with elasticity modulus E. In Figure 1, x^* and y^* are the Cartesian coordinates, $u^*(x^*, y^*, t^*)$ and $v^*(x^*, y^*, t^*)$ are the velocity components in x^* and y^* directions, respectively, and $p^*(x^*, y^*, t^*)$ is the pressure. The parameters ρ, ν, and p_a are the density, kinematic viscosity, and ambient or external pressure, respectively. The parameter p_o is the constant entrance pressure at $x^* = 0$, u_o the average entrance velocity, $\delta^*(x^*, t^*)$ the arbitrary position of the channel wall with respect to direction x^* and time t^*, and $\alpha(x^*, t^*)$ is the angle between the bending wall and the principal axis x^*. The asterisks $(^*)$ denote dimensional parameters that will be nondimensionalized later.

2.3. Governing Equations: Fluid Flow

The incompressible pulsatile flow is modeled using time-dependent, Navier-Stokes equations for Newtonian fluids coupled with the continuity equation. The equations are nondimensionalized using u_o, δ_o, p_o, and t_o as scales for velocities, lengths, pressure, and time, respectively. The nondimensional equation can be expressed thus:

$$\begin{aligned}
\frac{1}{\sqrt{\varepsilon}}\frac{\partial u}{\partial t} + u\frac{\partial u}{\partial x} + v\frac{\partial u}{\partial y} &= -\mathrm{Eu}\frac{\partial p}{\partial x} + \frac{1}{\mathrm{Re}}\left(\frac{\partial^2 u}{\partial x^2} + \frac{\partial^2 u}{\partial y^2}\right),\\
\frac{1}{\sqrt{\varepsilon}}\frac{\partial v}{\partial t} + u\frac{\partial v}{\partial x} + v\frac{\partial v}{\partial y} &= -\mathrm{Eu}\frac{\partial p}{\partial y} + \frac{1}{\mathrm{Re}}\left(\frac{\partial^2 v}{\partial x^2} + \frac{\partial^2 v}{\partial y^2}\right),\\
\frac{\partial u}{\partial x} + \frac{\partial v}{\partial y} &= 0,
\end{aligned} \tag{2.1}$$

where the nondimensional parameters $x = x^*/\delta_o$, $y = y^*/\delta_o$, $u = u^*/u_o$, $v = v^*/u_o$, $t = t^*/t_o\sqrt{\varepsilon}$, $t_o = \delta_o/u_o$ is the time scale, $\mathrm{Eu} = p_o/\rho {u_o}^2$, and $\mathrm{Re} = u_o\delta_o/\nu$ are Euler number and

Reynolds number, respectively, and $\delta_o/l^* \ll 1$, $\alpha_{\max} \ll 1$. The transmural pressure p is

$$p(x,y,t) = \frac{p_a - p^*(x^*,y^*,t^*)}{p_o}, \tag{2.2}$$

where p_o and p_a are the reference and atmospheric pressures, respectively.

The above Navier-Stokes equations will be simplified using the following assumptions: the stenosed segment of the channel is relatively long, $(\delta_o/l^* \ll 1)$, and the maximum angle of the slope of the stenosis with respect to the x^*-axis $\alpha_{\max} \ll 1$. The latter two conditions imply gradual change of the internal diameter of the channel along the principal axis. The relatively small inclination of the stenosis implies that all the physical quantities related to the structure will also be subject to very small variation in the direction of the principal axis. The flow is assumed to be fully developed throughout the channel. Thus the velocity component in the flow direction is large compared to the traverse component.

We translate small variations by introducing a coordinate $\xi = \varepsilon x$ and write the transverse velocity component in the form $v = \varepsilon V(\xi, y, t)$, where $V = O(1)$ and $0 < \varepsilon \ll 1$ will be defined later. We also assume that $\delta_o/l^* = O(\varepsilon)$ and $\alpha_{\max} = O(\varepsilon)$, $p(x,y,t)$, the space and time-varying transmural pressure (outer atmospheric pressure minus inner fluid pressure) is much smaller than the reference pressure p_o which is on the order 10^5 Pa [20]. We assume that the transmural pressure is transmitted through the wall alone. This condition can be formulated as $p = \varepsilon^n P(\xi, y, t)$, $P = O(1)$, where the parameter $n > 1$ will be defined later.

In terms of the new parameters, the Navier-stokes and continuity equations become

$$\begin{aligned}
&\frac{1}{\sqrt{\varepsilon}}\frac{\partial u}{\partial t} + \varepsilon\left(u\frac{\partial u}{\partial \xi} + V\frac{\partial u}{\partial y}\right) = -\varepsilon^{n+1}\mathrm{Eu}\frac{\partial P}{\partial \xi} + \frac{1}{\mathrm{Re}}\left(\varepsilon^2\frac{\partial^2 u}{\partial \xi^2} + \frac{\partial^2 u}{\partial y^2}\right),\\
&\frac{\varepsilon}{\sqrt{\varepsilon}}\frac{\partial V}{\partial t} + \varepsilon^2\left(u\frac{\partial V}{\partial \xi} + V\frac{\partial V}{\partial y}\right) = -\varepsilon^{n}\mathrm{Eu}\frac{\partial P}{\partial y} + \frac{\varepsilon}{\mathrm{Re}}\left(\varepsilon^2\frac{\partial^2 V}{\partial \xi^2} + \frac{\partial^2 V}{\partial y^2}\right),\\
&\frac{\partial u}{\partial \xi} + \frac{\partial V}{\partial y} = 0.
\end{aligned} \tag{2.3}$$

We consider the flow to be lubrication type, that is, the fluid is flowing very slowly and frictional forces are larger than inertial forces. The latter assumption implies that Reynolds number is low. In order to exploit the lubrication approximation, we make the following substitutions into (2.3):

$$\frac{1}{\mathrm{Eu}} = \varepsilon^{n+1}, \qquad \frac{1}{\mathrm{Re}} = \lambda = O\left(\varepsilon^k\right), \tag{2.4}$$

where $0 < k < 1$ and $\mathrm{Re} = O(1)$.

Keeping terms of up to order ε^2, we obtain

$$\frac{1}{\sqrt{\varepsilon}}\frac{\partial u}{\partial t}+\varepsilon\left(u\frac{\partial u}{\partial \xi}+V\frac{\partial u}{\partial y}\right)=-\frac{\partial P}{\partial \xi}+\lambda\frac{\partial^2 u}{\partial y^2}+O\left(\varepsilon^2\right), \tag{2.5}$$

$$\sqrt{\varepsilon}\frac{\partial V}{\partial t}=-\frac{1}{\varepsilon}\frac{\partial P}{\partial y}+O\left(\varepsilon^2\right), \tag{2.6}$$

$$\frac{\partial u}{\partial \xi}+\frac{\partial V}{\partial y}=0. \tag{2.7}$$

Equations (2.5), (2.6), and (2.7) have to be solved subject to the boundary conditions

$$\begin{aligned} y=\delta(t,\xi):\ & u=0, \qquad V=\frac{\partial \delta^*}{\partial t^*}=\frac{1}{\varepsilon^{3/2}}\frac{\partial \delta}{\partial t},\\ y=0:\ & \frac{\partial u}{\partial y}=\frac{\partial^3 u}{\partial y^3}=\frac{\partial^4 u}{\partial y^4}=\cdots=0, \qquad V=0. \end{aligned} \tag{2.8}$$

Our main goal is to obtain the nondimensional pressure distribution P in the channel wall. In order to achieve this goal, we first solve (2.5) for P thus

$$P(t,\xi,y)=\widehat{P}(t,y)-\int_0^{\xi}\left\{\lambda\frac{\partial^2 u}{\partial y^2}-\frac{1}{\sqrt{\varepsilon}}\frac{\partial u}{\partial t}-\varepsilon\left(u\frac{\partial u}{\partial \xi}+V\frac{\partial u}{\partial y}\right)\right\}d\varsigma, \tag{2.9}$$

where $\widehat{P}(t,y)$ is an arbitrary function of integration.

Taking into account the small ratio of radius to length and the parabolic profile along the flow direction, we assume that fluid velocity in the horizontal direction is given by

$$u(\xi,y,t)=\frac{3}{2}U\left(1-\frac{y^2}{\delta^2}\right), \tag{2.10}$$

where $U(t,\xi)$ is the cross-sectional average velocity. The latter is calculated as follows. First, we integrate the continuity equation (2.7) from 0 to y and obtain

$$V(t,\xi,y)=-\frac{3}{2}\frac{\partial U}{\partial \xi}\left(y-\frac{y^3}{3\delta^2}\right)-\frac{y^3}{\delta^3}\frac{\partial \delta}{\partial \xi}U+\overline{C}(t,\xi), \tag{2.11}$$

where $C(t,\xi)$ is an arbitrary function of integration.

By imposing the relevant boundary conditions on V that is (2.8), we obtain

$$\begin{aligned} &\overline{C}(t,\xi)=0,\\ &\frac{1}{\varepsilon^{3/2}}\frac{\partial \delta}{\partial t}+\frac{\partial U}{\partial \xi}\delta+\frac{\partial \delta}{\partial \xi}U=0. \end{aligned} \tag{2.12}$$

Thus

$$U = \frac{1}{\delta}\left(\theta(t) - \frac{1}{\varepsilon^{3/2}}\int_0^{\xi}\delta_t(t,z)dz\right), \tag{2.13}$$

where θ is an arbitrary function of integration and δ_t denotes $\partial\delta/\partial t$.

Next we substitute (2.10), (2.11), and (2.13) back into (2.9) giving

$$\begin{aligned} P(t,\xi,y) = \widehat{P}(t,y) - \int_0^{\xi}\Bigg\{ & \lambda\left(-3U\frac{y}{\delta^2}\right) - \frac{1}{\sqrt{\varepsilon}}\left[\frac{3}{2}\frac{\partial U}{\partial t}\left(1-\frac{y^2}{\delta^2}\right) + 3\frac{y^2}{\delta^3}\frac{\partial\delta}{\partial t}U\right] \\ & - \varepsilon\left[\frac{3}{2}U\left(1-\frac{y^2}{\delta^2}\right)\left(\frac{3}{2}\frac{\partial U}{\partial t}\left(1-\frac{y^2}{\delta^2}\right) + 3\frac{y^2}{\delta^3}\frac{\partial\delta}{\partial t}U\right)\right. \\ & \left. + \left(-\frac{3}{2}\frac{\partial U}{\partial\xi}\left(y-\frac{y^3}{3\delta^2}\right) - \frac{y^3}{\delta^3}\frac{\partial\delta}{\partial\xi}U\right)\left(-3U\frac{y}{\delta^2}\right)\right]\Bigg\}d\varsigma. \end{aligned} \tag{2.14}$$

In order to determine $\widehat{P}(t,y)$, we solve (2.6) for P. Then, we substitute the P obtained into (2.14) and obtain after some manipulations,

$$\begin{aligned} \widehat{P}(t,y) = \int_0^{\xi}\Bigg\{ & \lambda\left(-3U\frac{y}{\delta^2}\right) - \frac{1}{\sqrt{\varepsilon}}\left[\frac{3}{2}\frac{\partial U}{\partial t}\left(1-\frac{y^2}{\delta^2}\right) + 3\frac{y^2}{\delta^3}\frac{\partial\delta}{\partial t}U\right] \\ & - \varepsilon\left[\frac{3}{2}U\left(1-\frac{y^2}{\delta^2}\right)\left(\frac{3}{2}\frac{\partial U}{\partial t}\left(1-\frac{y^2}{\delta^2}\right) + 3\frac{y^2}{\delta^3}\frac{\partial\delta}{\partial t}U\right)\right. \\ & \left. + \left(-\frac{3}{2}\frac{\partial U}{\partial\xi}\left(y-\frac{y^3}{3\delta^2}\right) - \frac{y^3}{\delta^3}\frac{\partial\delta}{\partial\xi}U\right)\left(-3U\frac{y}{\delta^2}\right)\right]\Bigg\}d\varsigma - \varepsilon^{3/2}\int_0^{y}\frac{\partial V}{\partial t}dy' + \breve{P}(t), \end{aligned} \tag{2.15}$$

where $\breve{P}(t)$ is an arbitrary function of t.

Finally, by substituting (2.15) back into (2.14) and solving the resulting equation, we obtain the general form of the pressure distribution written as

$$\begin{aligned} & P(t,\xi,y) \\ & = \breve{P}(t) + \varepsilon^{3/2}\left[\frac{3}{2}\frac{\partial^2 U}{\partial t\partial\xi}\left(\frac{y^2}{2} - \frac{y^4}{12\delta^2}\right) + \frac{y^4}{4\delta^3}\frac{\partial\delta}{\partial t}\frac{\partial U}{\partial\xi} - \frac{3}{4}\frac{y^4}{\delta^4}\frac{\partial\delta}{\partial t}\frac{\partial\delta}{\partial\xi}U + \frac{y^4}{4\delta^3}\frac{\partial^2\delta}{\partial t\partial\xi}U + \frac{y^4}{4\delta^3}\frac{\partial U}{\partial t}\frac{\partial\delta}{\partial\xi}\right]. \end{aligned} \tag{2.16}$$

The nondimensional pressure distribution over the stenosed surface ($y = \delta$) is then

$$P(t,\xi,y=\delta) = \breve{P}(t) + \varepsilon^{3/2}\left[\frac{5}{8}\frac{\partial^2 U}{\partial t\partial\xi}\delta^2 + \frac{\delta}{4}\frac{\partial\delta}{\partial t}\frac{\partial U}{\partial\xi} - \frac{3}{4}\frac{\partial\delta}{\partial t}\frac{\partial\delta}{\partial\xi}U + \frac{\delta}{4}\frac{\partial^2\delta}{\partial t\partial\xi}U + \frac{\delta}{4}\frac{\partial U}{\partial t}\frac{\partial\delta}{\partial\xi}\right], \tag{2.17}$$

where U is given by (2.13) and $\breve{P}(t)$ is an arbitrary function.

By substituting (2.13) into (2.17) we finally obtain the pressure distribution over the stenosed surface as

$$\begin{aligned} P(t,\xi,\delta) = \breve{P}(t) + \frac{1}{4}\varepsilon^{3/2}\Bigg\{ & \frac{5}{2}\frac{\partial^2}{\partial t\partial\xi}\left[\frac{1}{\delta}\left(\theta(t) - \frac{1}{\varepsilon^{3/2}}\int_0^\xi \delta_t(t,z)dz\right)\right]\delta^2 \\ & + \delta\frac{\partial\delta}{\partial t}\frac{\partial}{\partial\xi}\left[\frac{1}{\delta}\left(\theta(t) - \frac{1}{\varepsilon^{3/2}}\int_0^\xi \delta_t(t,z)dz\right)\right] \\ & - \frac{3}{\delta}\frac{\partial\delta}{\partial\xi}\frac{\partial\delta}{\partial t}\left(\theta(t) - \frac{1}{\varepsilon^{3/2}}\int_0^\xi \delta_t(t,z)dz\right) \\ & + \frac{\partial^2\delta}{\partial t\partial\xi}\left(\theta(t) - \frac{1}{\varepsilon^{3/2}}\int_0^\xi \delta_t(t,z)dz\right) \\ & + \delta\frac{\partial\delta}{\partial\xi}\frac{\partial}{\partial t}\left[\frac{1}{\delta}\left(\theta(t) - \frac{1}{\varepsilon^{3/2}}\int_0^\xi \delta_t(t,z)dz\right)\right]\Bigg\}. \end{aligned} \tag{2.18}$$

Note that pressure is evaluated at points which happen to be also the limits of integration. Therefore, care must be taken when choosing the numerical method to evaluate (2.18). Here, we define a new variable

$$B = \theta(t) - \frac{1}{\varepsilon^{3/2}}\int_0^\xi \delta_t(t,z)dz \tag{2.19}$$

such that B is completely defined by

$$\begin{gathered} \frac{\partial B(t,\xi)}{\partial\xi} = -\frac{1}{\varepsilon^{3/2}}\frac{\partial\delta(t,z)}{\partial t}, \\ B(t,0) = \theta(t). \end{gathered} \tag{2.20}$$

2.4. Governing Equations: Artery Wall

The artery wall configuration is driven by hemodynamic stresses acting on its surface. The elastic wall configuration is solved as a plate. We start by applying Newton's second law of motion to the surface element presented in Figure 2. It should be remarked that α in this

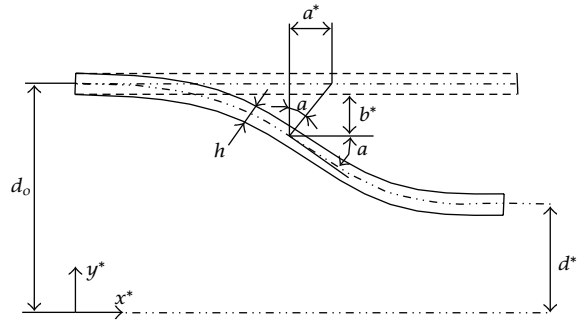

Figure 2: Segment of channel wall.

section represents the angle of wall inclination as illustrated in Figure 2. Newton's second law is expressed by

$$\sum \vec{F} = M \cdot \vec{\dot{V}}, \tag{2.21}$$

where $\vec{F}$ is the external force vector, and M and $\vec{\dot{V}}$ are mass and acceleration vector, respectively.

The transverse component of (2.21) is obtained through force balance on artery wall material element (see Figure 1) in the transverse direction, thus

$$\tau_w \sin(\alpha) dx^* - (F + dF)\sin(\alpha + d\alpha) + F\sin(\alpha) - (p_a - p^*)dx^* + V + dV - V = h\rho dx^* \frac{d^2 b^*}{dt^{*2}}, \tag{2.22}$$

where τ_w is the shear stress over the inner face of the wall, F is the magnitude of the force at inclination α, $F + dF$ is the magnitude of the force at inclination $\alpha + d\alpha$ as a result of the bend, and ρ the material density

$$F = \sigma_{x^*} h, \quad V = -\frac{dM}{dx^*}, \qquad M = \int_{-h/2}^{h/2} \sigma_{x^*} y^* dy^*, \ \sigma_{x^*} = \frac{E}{1-\nu^2}\varepsilon_{x^*}. \tag{2.23}$$

Based on Karman's nonlinear shell theory [21], Djordjevic and Vukobratovic [13] have shown that the finite strain component in the axial direction takes the form:

$$\varepsilon_{x'} = \frac{da^*}{dx^*} + \frac{1}{2}\left[\left(\frac{da^*}{dx^*}\right)^2 + \left(\frac{db^*}{dx^*}\right)^2\right]. \tag{2.24}$$

We assume that α is small. Hence $\tan\alpha = -db^*/dx^*$, $\sin(\alpha) \cong \alpha$ and $\sin(\alpha + d\alpha) \cong \alpha + d\alpha$. The latter approximation converts (2.22) into

$$-\tau_w \frac{db^*}{dx^*} + \frac{Eh}{1-\nu^2}\frac{d^2 b^*}{dx^{*2}}\varepsilon_{x^*} - \frac{Eh^3}{12(1-\nu^2)}\frac{d^4 b^*}{dx^{*4}} - (p_a - p^*) = h\rho\frac{d^2 b^*}{dt^{*2}} + \text{h.o.t}, \tag{2.25}$$

where the abbreviation h.o.t stands for Higher Order Terms. We may recast (2.25) into

$$T\frac{d^2b^*}{dx^{*2}} - D\frac{d^4b^*}{dx^{*4}} - \tau_w\frac{db^*}{dx^*} - \left(p_a - p^*\right) = h\rho\frac{d^2b^*}{dt^{*2}} + \text{h.o.t}, \tag{2.26}$$

where $D = Eh^3/12(1-\nu^2)$ and $T = (Eh/(1-\nu^2))\varepsilon_{x^*}$ are the bending stiffness and the longitudinal tension, respectively.

The axial component (X) of the equation of motion is similarly obtained through momentum balance on artery wall element in the axial direction,

$$-F\cos(\alpha) + (F+dF)\cos(\alpha+d\alpha) - \tau_w\cos(\alpha)dx^* + \left(p_a - p^*\right)\sin(\alpha) = h\rho\frac{d^2a^*}{dt^{*2}}dx^* + \text{h.o.t.} \tag{2.27}$$

Using the fact that α is small we obtain

$$\frac{dT}{dx^*} - \tau_w + \left(p_a - p^*\right)\frac{\partial b^*}{\partial x^*} = \rho h\frac{d^2a^*}{dt^{*2}}. \tag{2.28}$$

Now, we proceed to nondimensionalize equations (2.25) and (2.26) by introducing the following nondimensional variables:

$$x = \frac{x^*}{\delta_o}, \qquad a = \frac{a^*}{\delta_o}, \qquad b = \frac{b^*}{\delta_o}, \qquad a = \varepsilon A(t,\xi),\ \xi = \varepsilon x, \qquad t = \frac{1}{\sqrt{\varepsilon}}\frac{t^*}{t_o}, \qquad t_o = \frac{\delta_o}{u_o}. \tag{2.29}$$

In terms of the new variables, we have

$$\varepsilon_\xi = \varepsilon^2\left[\frac{dA}{d\xi} + \frac{1}{2}\left(\frac{\partial b}{\partial\xi}\right)^2\right] + O\left(\varepsilon^4\right). \tag{2.30}$$

Equations (2.25) and (2.26) become, respectively,

$$\begin{aligned}&\varepsilon^4\frac{E}{1-\vartheta^2}\frac{h}{\delta_o}\left[\frac{dA}{d\xi} + \frac{1}{2}\left(\frac{\partial b}{\partial\xi}\right)^2\right]\frac{\partial^2 b}{\partial\xi^2}\\ &\quad - \frac{E\varepsilon^4}{12(1-\vartheta^2)}\left(\frac{h}{\delta_o}\right)^3\frac{\partial^4 b}{\partial\xi^4} - \varepsilon^n P(t,\xi,y)p_o = \varepsilon^n p_o\frac{h}{\delta_o}\frac{d^2b}{dt^2} + O\left(\varepsilon^{n+1}\right),\end{aligned} \tag{2.31}$$

$$\varepsilon^3\frac{E}{1-\vartheta^2}\frac{h}{\delta_o}\frac{\partial}{\partial\xi}\left[\frac{dA}{d\xi} + \frac{1}{2}\left(\frac{\partial b}{\partial\xi}\right)^2\right] + O\left(2p_o\varepsilon^{n+1}\frac{h}{\delta_o}\right) = 0. \tag{2.32}$$

Integration of (2.32) yields

$$\frac{dA}{d\xi} + \frac{1}{2}\left(\frac{\partial b}{\partial \xi}\right)^2 = K(t). \tag{2.33}$$

Thus

$$\int_0^L \left(\frac{\partial b}{\partial \xi}\right)^2 d\xi = 2K(t)L, \tag{2.34}$$

where L is the nondimensional wall length.

Using the dominant balance in (2.31), we set

$$\varepsilon^4 \frac{E}{1-\vartheta^2}\frac{h}{\delta_o} = \varepsilon^n p_o. \tag{2.35}$$

Recall also that

$$\mathrm{Eu} = \frac{p_0 \delta_0^2 \lambda^2}{\rho \nu^2} = O(1). \tag{2.36}$$

Equations (2.35) and (2.36) imply that

$$n = -\left(1 + \frac{\ln\ \mathrm{Eu}}{\ln \varepsilon}\right), \qquad \varepsilon = \left[\frac{\rho \nu^2 (1-\vartheta^2)}{Eh\delta_0 \lambda^2}\right]^{1/5}. \tag{2.37}$$

Using (2.34), (2.22) can be rewritten as

$$K\frac{\partial^2 b}{\partial \xi^2} - \frac{1}{12}\left(\frac{h}{\delta_o}\right)^2 \frac{\partial^4 b}{\partial \xi^4} - P = \frac{h}{\delta_o}\frac{d^2 b}{dt^2}. \tag{2.38}$$

Recalling that $b = \delta - 1$, (2.38) may be transformed further to

$$K\frac{\partial^2 \delta}{\partial \xi^2} - \frac{1}{12}\left(\frac{h}{\delta_o}\right)^2 \frac{\partial^4 \delta}{\partial \xi^4} - P = \frac{h}{\delta_o}\frac{\partial^2 \delta}{\partial t^2}, \tag{2.39}$$

or equivalently

$$-{m_1}^2 \delta^{(\mathrm{IV})} + m_2 \delta^{(\mathrm{II})} - m_3 = 12 m_1 \ddot{\delta}, \tag{2.40}$$

where the superscripts and the overdot stand for differentiation with respect to ξ and t, and

$$m_1 = \frac{h}{\delta_o}, \qquad m_2 = 12K, \qquad m_3 = 12P. \tag{2.41}$$

In the next section, we describe the numerical methods used to solve the above governing equations.

2.5. Numerical Solution Procedure

The main issue with the wall governing equation (2.41) in the transient state is solving a single differential equation with two unknowns, including transmural pressure distribution P and wall deflection δ. Computation of the wall shape (wall deflection) at the next time step proceeds as follows. Knowing the wall shape at the initial time step (deflection distribution δ at the initial time), we solve the equation of the transmural pressure equation (2.18) for P. Then, at the next time step we solve the wall governing equation (2.39) for δ under the assumption that the time step Δt is small enough to apply $P|_{t=n} \approx P|_{t=n+1}$. Next, given the updated solution for δ, we can find the corresponding updated P, and so on until the final iteration in time.

We used the finite difference method [22, 23] to solve the transmural pressure equation (2.18) and governing equation (2.39). Specifically, the arterial wall was discretized into segments. Next, a node was placed between two consecutive segments. More than 100 nodes were distributed over the wall length. Then incremental numerical calculations were applied at each node.

For the differential terms included in the transmural pressure equation (2.18) and governing Equations (2.39), forward and central schemes [22] were used to solve time- and space-dependent terms, respectively. Also, the trapezoidal rule [23] was utilized for solving the integral term equation (2.19). Numerical accuracy was first assured by systematically increasing the number of nodes until the results became invariant with further increase. Then the numerical code was validated by comparing the predicted results for steady-state cases with available results from other studies that used different solution methods (Djordjevic and Vukobratovic [13] and Luo and Pedley [10]). Our predictions were qualitatively in agreement with those studies.

The solution procedure is initialized by first defining the shape of the stenotic arterial wall with a small slope in fulfillment of the lubrication theory. Next, with the imposed boundary conditions and numerical schemes in place, the transmural pressure is solved first at all the nodes of the wall. The matrix containing the transmural pressure at each node is inserted into the governing equation (2.39). Then the latter equation is solved for all the nodes at once using the implicit Thomas algorithm [22]. The results obtained provide the new location distribution of nodes at the current time step. Finally, new configuration of the arterial wall is used to update the initial configuration for the next time step. The procedure continues in time until the input number of time steps is achieved or the solution becomes unstable. Stability is controlled by the Courant number C, defined as $U_{\max} * \Delta t/\Delta x < C$, where $C = 1$ and $U_{\max}$ is the maximum flow velocity. All the computations are performed using Matlab 6.5 software.

3. Results

In this section, we present the results and discuss the effect of the control parameters, including inlet velocity U_o, (or equivalently the Reynolds number, Re), inlet transmural pressure P_t, and arterial wall thickness h. The other parameters are kept constant, including arterial segment length L, Elastic modulus E, Poisson ratio ϑ, fluid kinematic viscosity, ν,

Table 1: Input data utilized in this study.

L (mm)	δ_o (mm)	U_o-m/s	Re	P_t (Pa)	ν(m^2/s)	E-N/m^2	γ	h-mm	P_o (Pa)	ϑ
100	3	0.1–0.3	3.2–9.6	180–210	$3.6*10^{-6}$	$5.6*10^5$	10%	0.7–0.9	10^5	0.49

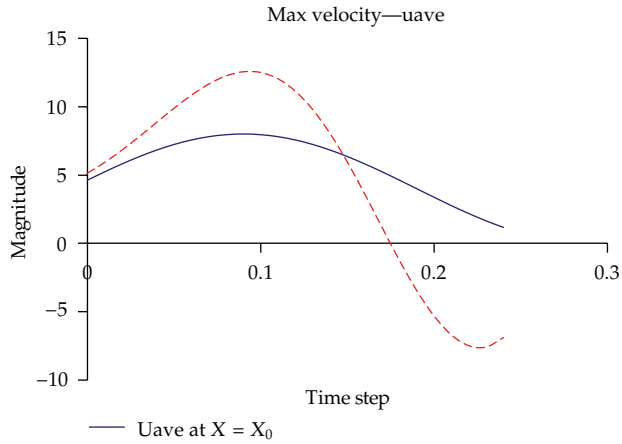

Figure 3: Average velocity profile of pulsatile flow applied at the inlet and midlength of segment.

initial wall deflection relative to nominal radius, γ, and reference pressure P_o which is taken as atmospheric. The input data utilized in this study are presented in Table 1, in which δ_o is the segment radius. These input values have been selected based on previous work and established data on human coronary artery [24–26]. The segment length $L = 100$ mm, the nominal diameter $\delta_o = 3$ mm, and inlet velocity (and correspondingly, the Reynolds number range) are typical in straight sections of adult human coronary arteries [24, 25]. The Young's modulus (E) and Poison ratio (ϑ) are elastic properties of the wall and are similarly chosen to be typical of human coronary arteries [24–26]. It should however be noted that the elastic properties may vary depending on the extent of disease. The viscosity is a well-established property of blood of normal hematocrit [25]. The transmural pressure P_t, wall thickness h, and inlet velocity U_o are control parameters which do not necessarily have to be constant in a single artery. For example, the thickness h may vary depending on the type of plaque (focal or distributed) and location of plaque and segment of the artery being considered. Inlet pressure depends on the blood pressure which may be patient specific. Inlet velocity and pressure similarly depend on the location of the coronary artery being considered relative to the aorta. The control parameters could therefore be varied in a parametric analysis as done in this paper to investigate the effect of blood pressure, intima thickness, and flow rate. The ramge of values used for the study are typical of human coronary arteries [24–26].

In order to compare our results with the steady-state solution of Djordjevic and Vukobratovic [13], we applied the parabolic profile velocity of (2.10) at the tube inlet. Figure 3 shows the time-dependent cross-sectional average velocity $U(t, \xi)$ (2.13) calculated at the inlet and at midlength of segment. We applied oscillatory flow velocity to simulate pulsatile blood flow in a coronary artery. It should be noted that the average velocity varies not only with time but also space as fluid flows through the constricted segment of the channel.

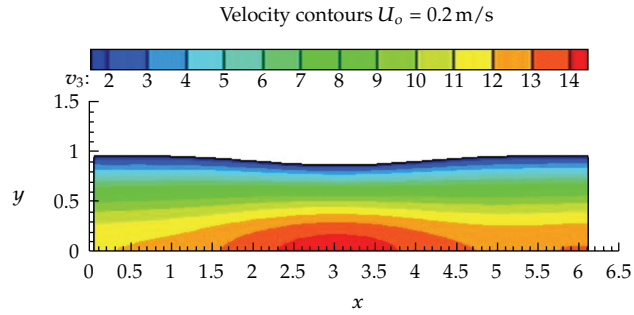

Figure 4: Typical velocity profile at time $t = 0.1$ shows that the flow is fully developed throughout the channel.

3.1. Velocity Profile

Figure 4 shows typical predicted profile of magnitude of velocity (inlet velocity $U_o = 0.2\,\mathrm{m/s}$, $t = 0.1\,\mathrm{s}$) in the tube in which the y-axis represents the radial direction from centerline ($y = 0$) to the wall (e.g., $y = 1$ at inlet), and x the longitudinal direction from inlet ($x = 0$) to the outlet ($x = 6$). Minimum velocity is represented with blue in the color code and maximum with red. The result indicates that at every axial location (x) the velocity varies from a minimum at the wall to maximum at the centerline, in the consensus of a developed parabolic profile in a tube. The variation in velocity is a result of fluid viscosity, which allows the velocity relative to the wall to be zero, while reaching a maximum at the axis of the channel. The largest velocity in the tube occurs at midlength between the inlet and the outlet sections where the tube is most constricted (i.e., minimum cross-sectional area), as expected, in order to satisfy mass conservation. These results while not novel, serve to validate the model as it correctly predicts the expected velocity profile in the tube.

3.2. Effect of Inlet Velocity

Figure 5(a) shows the predicted transmural pressure distribution along the tube for three inlet velocities $U_o = 0.1\,\mathrm{m/s}$ (thin blue line), $0.2\,\mathrm{m/s}$ (purple continuous line) and $0.3\,\mathrm{m/s}$ (red dash line). The Reynolds number ranges from 3.2 to 9.6, well within the lubrication theory regime assumed in the analysis. The other parameters such as transmural pressure at the inlet ($P_{to} = 180\,\mathrm{Pa}$), and wall thickness $h = 0.8\,\mathrm{mm}$, are kept constant. The corresponding wall shear stress distribution is presented in Figure 5(b). In general, the transmural pressure decreases (magnitude increases) from the inlet to the trough of the channel and then drops (magnitude increases) in the downstream tube expansion towards the outlet. The slight oscillation in pressure at the end of the segment may be attributed to artifacts of the numerical scheme in satisfying the imposed boundary condition at the tube ends. Figure 5(a) also shows that P_t is highest (magnitude is lowest) and is nearly uniform at the highest inlet velocity, $U_o = 0.3\,\mathrm{m/s}$. The coupling of Reynolds number (inlet velocity) to transmural pressure $p = \varepsilon^n P(\xi, y, t)$ of (2.2) is expressed directly through (2.37) for the parameters n and ε. Increasing the Re reduces the magnitude of the transmural pressure. Corresponding to the observed intramural pressure trend, Figure 5(b) shows that the wall shear stress is nearly uniform at the highest inlet velocity when the large flow momentum is sufficient to overcome the effect of tube constriction.

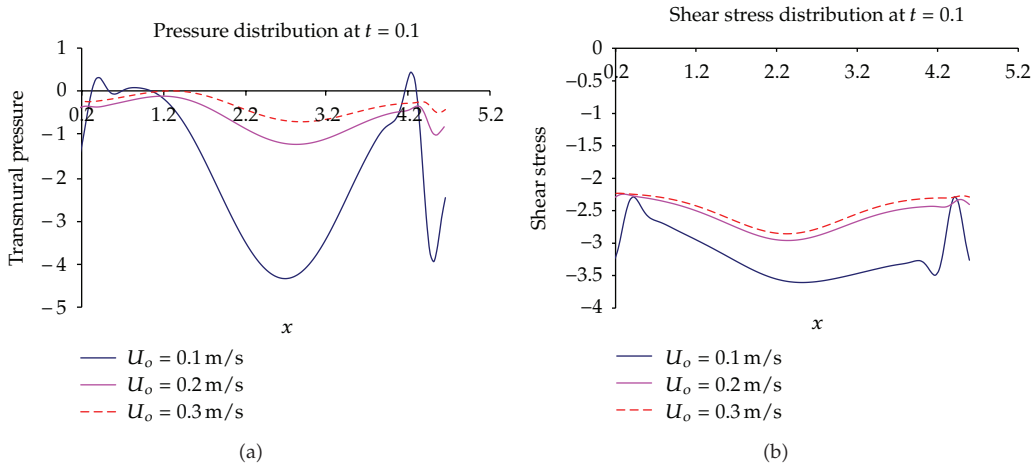

Figure 5: Intramural pressure distribution (a), and wall shear stress distribution (b) for inlet velocity $\mathbf{U_o}$ = 0.1 m/s, 0.2 m/s, 0.3 m/s.

Note that all the results presented in Figure 5 (as well as subsequent ones) are characterized by asymmetry between the tube inlet and outlet due to the effect of fluid flow. This observation is consistent with results obtained in previous studies [10, 27].

Figure 6 presents the transient wall deflection corresponding to the pressure and wall shear stress results of Figure 5 above, for inlet velocity U_o ranging from 0.1 to 0.3 m/s. In each of the plots, the direction of increasing time is from bottom to top. The results indicate that the amplitude of wall deflection decreases as Re increases. In other words, the wall progressively flattens out as Re increases, in the consensus of the previously observed flattening of the pressure curve (due to significant reduction in magnitude of transmural pressure) and wall shear stress curve at high Re in Figure 5. Figure 6 also shows the wall deflection is the highest towards the half length of the segment. This trend is consistent with the steady-state results of Djordjevic and Vukobratovic [13] and Luo and Pedley [10, 27]. There is significant wall oscillation, especially at the smallest Re. This wall oscillation, when considered in conjuction with the magnitude of the transmural pressure presented in Figure 5(a) suggests possible approach to breakdown in equilibrium.

3.3. *Effect of Inlet Transmural Pressure*

Figure 7(a) shows the predicted transmural pressure P_t at t = 0.1 s along the segment length for three inlet transmural pressures (P_{to} =180 Pa, 200 Pa, and 220 Pa). The Reynolds number Re = 6.4 and wall thickness h = 0.8 mm. The corresponding wall shear stress distribution is presented in Figure 7(b). The results indicate that increasing P_{to} reduces both the magnitude and longitudinal gradient of the transmural pressure along the tube. This finding is consistent with a previous steady state study [27] indicating that high P_{to} effectively results in a reduction of longitudinal tension in the membrane, or increase in the internal pressure. The net result is a flattening of the membrane as would be described below. The flattened wall in turn leads to a reduction in wall frication, translating to a reduction in wall shear stress as observed in Figure 7(b).

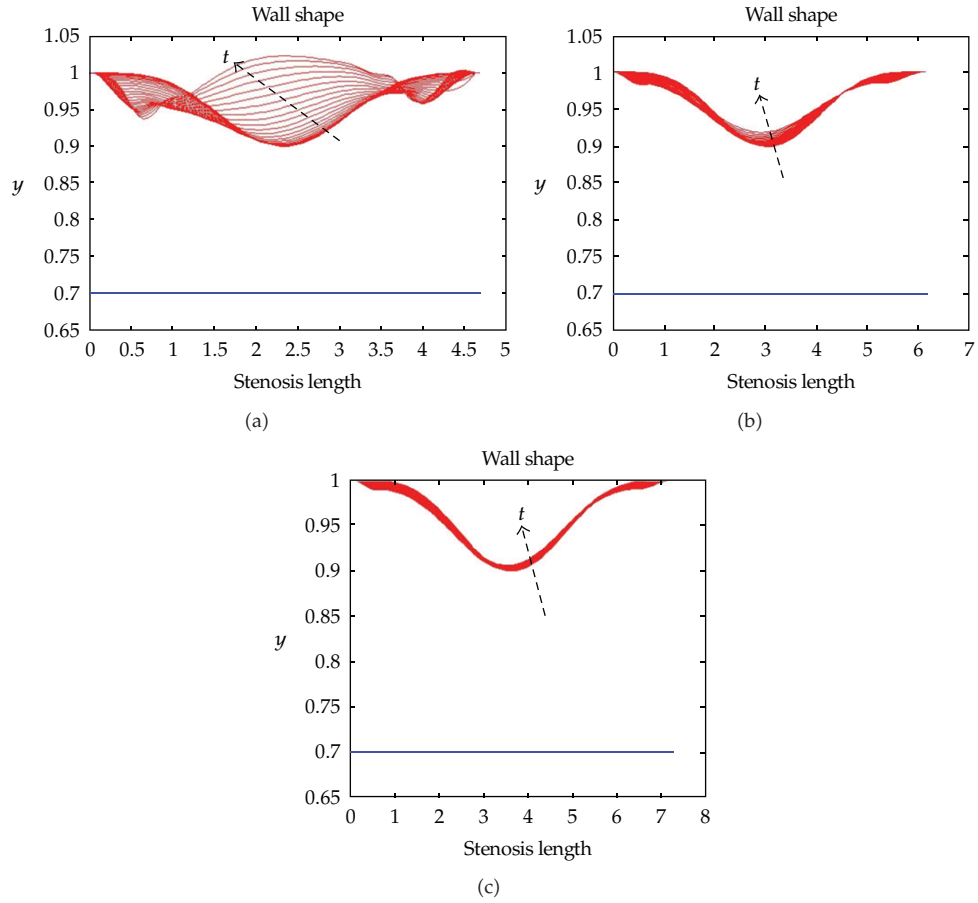

Figure 6: Wall shape for inlet velocity U_o of 0.1 m/s (a), 0.2 m/s (b), 0.3 m/s (c).

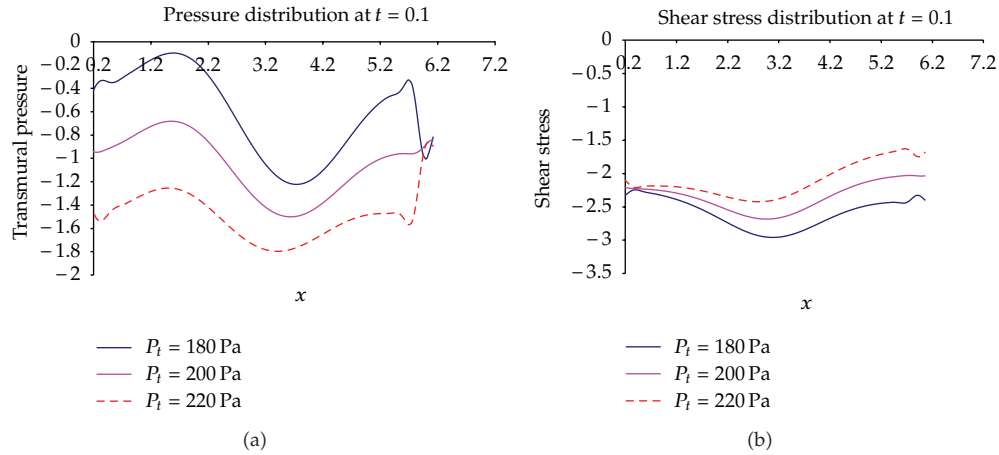

Figure 7: Distribution of pressure (a) and wall shear stress (b), for inlet transmural pressure of 180 Pa, 200 Pa and 220 Pa.

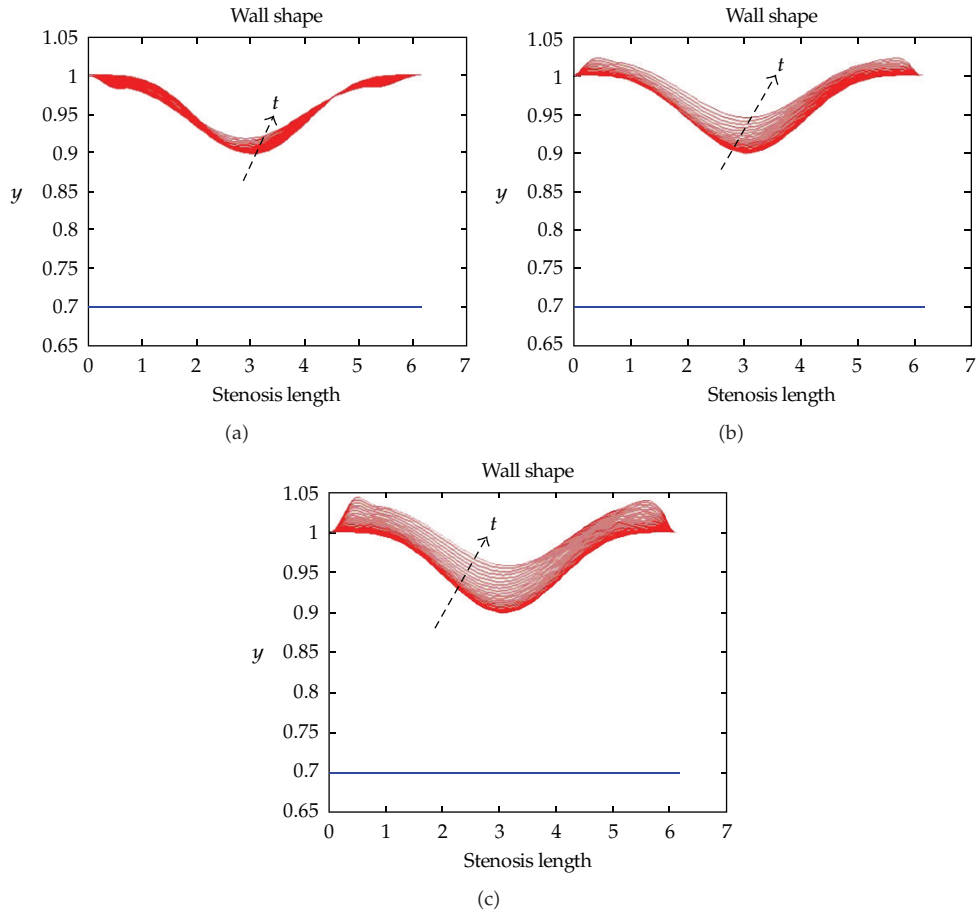

Figure 8: Wall shape for inlet transmural pressure, P_{to} = 180 Pa (a), 200 Pa (b), 220 Pa (c).

The predicted transient wall deflections corresponding to the results of Figure 7 are presented in Figure 8, with (a) representing P_{to} = 180 Pa, (b) 200 Pa and (c) 220 Pa. Increasing P_{to} results in outward movement of membrane (i.e., increased wall deflection). This trend is consistent with the increase in internal pressure resulting from increased P_{to} and has also been observed in a previous steady-state study [13]. A bulge is predicted at both the upstream and downstream ends of the segment. The former is consistent with that observed in a previous study utilizing higher initial wall constriction [27]. The second downstream bulge, observed here, is not surprising in such a situation of high transmural pressures coupled with small wall constriction. Specifically, the small initial wall deflection implies some degree of symmetry at both ends of the segment.

3.4. *Effect of Wall Thickness, h*

Figure 9(a) shows the predicted transmural pressure, P_t, at 0.1 s along the tube for three wall thicknesses h = 0.7 mm, 0.8 mm, and 0.9 mm. The inlet parameters are kept constant at Re = 6.4, and P_{to} = 180 Pa. The corresponding wall shear stress distribution is presented in

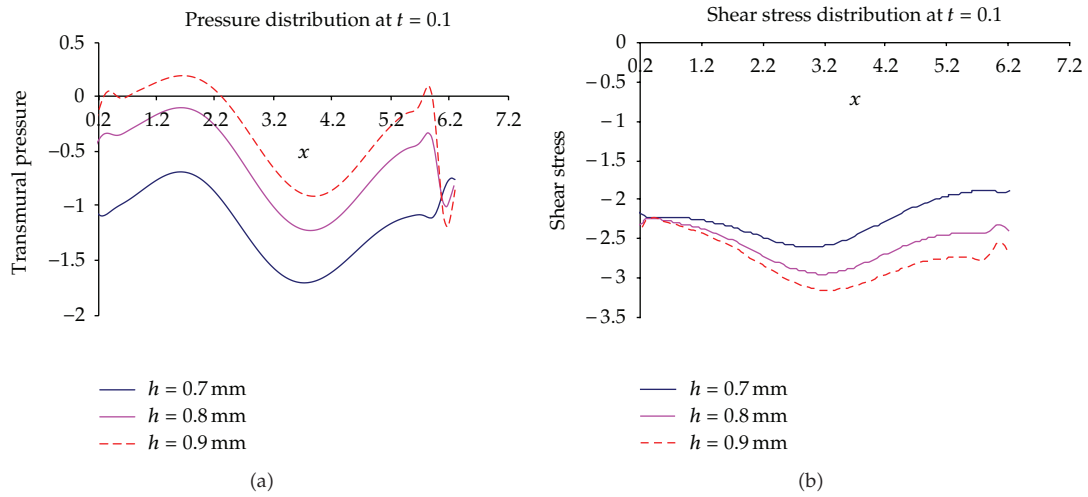

Figure 9: Transmural pressure distribution (a) and wall shear stress distribution (b) for wall thickness varying from 0.7 mm to 0.9 mm.

Figure 9(b). The results show that increase in h reduces the magnitude of the transmural pressure, P_t. This decrease in P_t increases the wall shear stress, progressively destabilizes the membrane, and may ultimately lead to its collapse as described below.

Figure 10 presents the predicted transient wall deflections as a function of the wall thickness, h. Increase in the thickness from 0.7 mm to 0.8 mm produces a reduction in wall deflection. This trend has also been predicted in a previous steady-state analysis [13]. The present transient analysis shows that further increase in h from 0.8 mm to 0.9 mm dramatically alters the trend. Specifically, although the deflection is still reduced at the trough, the crests now exhibit larger deflections than those for $h = 0.7$ mm and 0.8 mm. The large crest deflections may be attributed to significant increase in the bending force at large h. Note that the wall thickness h appears in the 4th order bending force term of the integrodifferential equation (2.39). This being the dominant term of the equation implies that any slight change in the bending force due to change in h will have significant effect on the wall configuration as observed in Figure 10.

4. Conclusion

A transient analytical model based on the lubrication theory has been developed to study flow-structure interaction in a two-dimensional constricted distensible tube with compliant wall. Previous analytical studies have focused on the steady state. The long-term objective of the present study is to use the transient model developed to provide a relatively simple means of investigating the essential features of stenosed (diseased) vascular remodeling. Such remodeling occurs due to the elasticity of the walls and the pulsatile fluid flow through the vessel. The resulting wall shear stress pattern and wall dynamics have been implicated in the genesis of vascular diseases such as atherosclerosis, as well as plaque rupture that causes to myocardial infarction (heart attack) and may ultimately lead to death. In the present model, the Karman plate theory in the transient mode is used to obtain expressions for the transmural pressure in order to derive a single integrodifferential equation for the wall

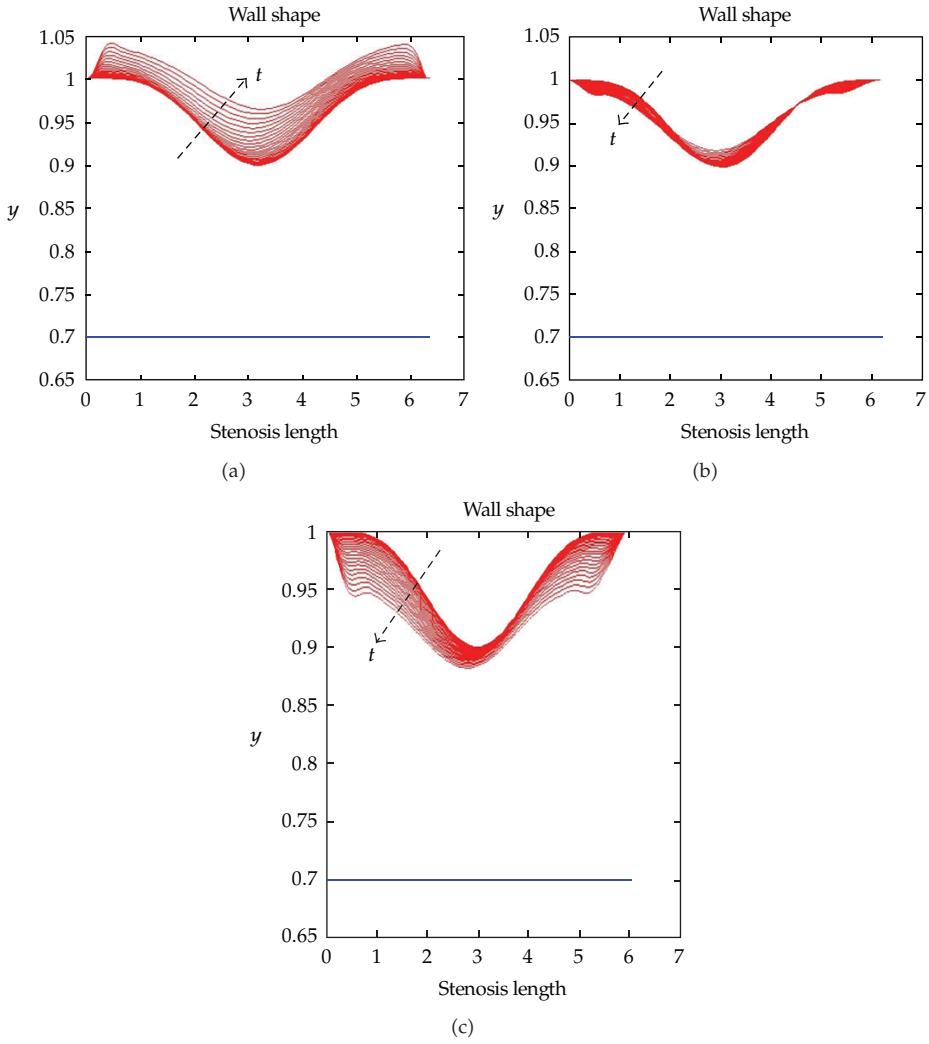

Figure 10: Predicted wall shape for wall thickness $h = 0.7$ mm (a), 0.8 mm (b), and 0.9 mm (c).

behavior. The equation was then solved by the finite difference method. Parametric studies were conducted on the effect of three parameters: Reynolds number, Re (or correspondingly the inlet velocity, U_o), inlet transmural pressure, P_{to}, and wall thickness, h.

The primary findings of the analytical study for the specific conditions considered may be summarized thus.

(i) Increase in Reynolds number while keeping P_{to} and h constant results in a reduction in the magnitude of the transmural pressure. This reduction in P_t in turn results in a reduction in both the wall deflection and wall shear stress. The wall is most vulnerable to oscillations at low Re when the other system parameters (P_{to}, h) are fixed. The wall deflections are also generally larger upstream of the trough (minimum diameter at midlength) than downstream.

(ii) Increase in the inlet transmural pressure P_{to} while keeping h and Re constant causes a reduction in longitudinal tension and a flattening of the wall. This trend results in a reduction in the wall friction and wall shear stress.

(iii) Increase in wall thickness h while keeping P_{to} and Re constant reduces the wall deflections for h below a threshold (here $h = 0.8\,\text{mm}$). Increasing h beyond this threshold leads to large deflection especially at the ends and possible breakdown of the wall. This collapse of the membrane is due to large bending force that develops at the ends at large wall thickness.

The results at specific time duration seem to agree generally with previous steady-state results [10, 12, 13]. They are also generally in the consensus of medical studies on cardiovascular diseases. For example, the low shear stress resulting from increase in the inlet transmural pressure P_{to} implies that the latter may indeed promote atherogenesis. The latter has been found to be focal in coronary arteries and located in regions of low wall shear stress. These are also regions of platelet accumulation. The observed deflection is larger upstream than downstream of the trough. This trend is consistent with observations that plaques typically rupture at upstream shoulders, that is, upstream of the region of minimum vascular diameter. Increase in wall thickness may be directly related to intimal thickening due to vascular inflammation. The present results indicate that such thickening may lead to possible breakdown or rupture of the wall and plaque especially near the ends. Plaque rupture causes thrombosis and may lead to heart attack and death.

Our analysis has demonstrated that with proper assumptions the transient model can be used to study the unsteady flow-structure interaction phenomena in a constricted compliant channel. The results obtained from the investigation are consistent with previous analytical studies [10, 12, 13]. The study is currently limited to system behavior in the relatively low Reynolds number range 3.2 to 9.6 in order to simulate flow in the coronary arteries that are most vulnerable to vascular plaque growth and rupture. Subsequent efforts will be extended to higher Reynolds numbers in order to investigate other interesting phenomena such as self-excited oscillations for direct comparison with available experimental data that were conveniently conducted at high Re. In addition, it is desirable to improve the model by extending to larger initial membrane curvature.

Next, it would be interesting to perform stability analysis of the improved model to investigate membrane self-excited oscillation [10, 27, 28]. The investigation will help to optimize the model by determining the role each controlling parameter plays in order to focus on the most important one in analyzing the fluid-structure phenomena. Ultimately, the model would be extended to investigate the fully coupled three-dimensional model. The investigation of the fully three-dimensional geometry [10, 27] in order to investigate the subtleties compared to the 2D model considered in the present study. Such subtleties include snap-through buckling of the tube wall, flow division into multiple lobes which remains open during the buckling, and buckling with higher circumferential wave numbers for increased upstream pressure.

References

[1] J. B. Grotberg and O. E. Jensen, "Biofluid mechanics in flexible tubes," *Annual Review of Fluid Mechanics*, vol. 36, pp. 121–147, 2004.

[2] M. Heil, "Stokes flow in collapsible tubes: computation and experiment," *Journal of Fluid Mechanics*, vol. 353, pp. 285–312, 1997.

[3] A. I. Katz, Y. Chen, and A. H. Moreno, "Flow through a collapsible tube. Experimental analysis and mathematical model," *Biophysical Journal*, vol. 9, no. 10, pp. 1261–1279, 1969.
[4] W. A. Conrad, "Pressure-flow relationships in collapsible tubes," *IEEE Transactions on Biomedical Engineering*, vol. 16, no. 4, pp. 284–295, 1969.
[5] R. D. Kamm and T. J. Pedley, "Flow in collapsible tubes: a brief review," *Journal of Biomechanical Engineering*, vol. 111, no. 3, pp. 177–179, 1989.
[6] R. L. Panton, *Incompressible Flow*, John Wiley & Sons, 2nd edition, 1995.
[7] A. H. Shapiro, "Steady flow in collapsible tubes," *Journal of Biomechanical Engineering*, vol. 99, no. 3, pp. 126–147, 1977.
[8] M. P. Rast, "Simultaneous solution of the Navier-Stokes and elastic membrane equations by a finite element method," *International Journal for Numerical Methods in Fluids*, vol. 19, pp. 1115–1135, 1994.
[9] T. W. Lowe and T. J. Pedley, "Computation of stokes flow in a channel with a collapsible segment," *Journal of Fluids and Structures*, vol. 9, no. 8, pp. 885–905, 1995.
[10] X. Y. Luo and T. J. Pedley, "A numerical simulation of unsteady flow in a two-dimensional collapsible channel," *Journal of Fluid Mechanics*, vol. 314, pp. 191–225, 1996.
[11] J. J. Shin, *The numerical simulation of flow through collapsible channels*, Ph.D. thesis, MIT, 1996.
[12] T. J. Pedley, "Longitudinal tension variation in collapsible channels: a new mechanism for the breakdown of steady flow," *Journal of Biomechanical Engineering*, vol. 114, no. 1, pp. 60–67, 1992.
[13] V. D. Djordjevic and M. Vukobratovic, "On a steady, viscous flow in two-dimensional collapsible channels," *Acta Mechanica*, vol. 163, no. 3-4, pp. 189–205, 2003.
[14] M. Heil, *Large deformations of cylindrical shell conveying viscous flow*, Ph.D. thesis, University of Leeds, 1995.
[15] M. Heil and T. J. Pedley, "Large post-buckling deformations of cylindrical shells conveying viscous flow," *Journal of Fluids and Structures*, vol. 10, no. 6, pp. 565–599, 1996.
[16] T. J. Pedley, *Fluid Mechanics of Large Blood Vessels*, Cambridge University Press, Cambridge, UK, 1980.
[17] V. Shankar and V. Kumaran, "Stability of wall modes in fluid flow past a flexible surface," *Physics of Fluids*, vol. 14, no. 7, pp. 2324–2338, 2002.
[18] A. D. Shah and J. D. Humphrey, "Finite strain elastodynamics of intracranial saccular aneurysms," *Journal of Biomechanics*, vol. 32, no. 6, pp. 593–599, 1999.
[19] D. W. Nicholson, *Finite Element Analysis, Thermomechanics of Solids*, CRC Press, Boca Raton, Fla, USA, 2003.
[20] S. Kobayashi and D. Tsunoda, "Flow and compression in arterial models of stenosis with lipid core," in *Proceedings of ASME Summer Bioengineering Conference*, pp. 497–498, 2003.
[21] T. M. Atanackovic and A. Guran, *Theory of Elasticity for Scientists and Engineers*, Birkhäuser, Boston, Mass, USA, 2000.
[22] J. Tannehill, D. Anderson, and R. Pletcher, *Computational Fluid Mechanics and Heat Transfer*, Taylor & Francis, 2nd edition, 1997.
[23] S. Chapra and R. Canale, *Numerical Methods for Engineers with Software and Programming Applications*, MacGraw-Hill, Boston, Mass, USA, 2002.
[24] M. Bathe and R. D. Kamm, "A fluid-structure interaction finite element analysis of pulsatile blood flow through a compliant stenotic artery," *Journal of Biomechanical Engineering*, vol. 121, no. 4, pp. 361–369, 1999.
[25] V. A. Nosovitsky, O. J. Ilegbusi, J. Jiang, P. H. Stone, and C. L. Feldman, "Effects of curvature and stenosis-like narrowing on wall shear stress in a coronary artery model with phasic flow," *Computers and Biomedical Research*, vol. 30, no. 1, pp. 61–82, 1997.
[26] D. Tang, C. Yang, S. Kobayashi, J. Zheng, and R. P. Vito, "Effect of stenosis asymmetry on blood flow and artery compression: a three-dimensional fluid-structure interaction model," *Annals of Biomedical Engineering*, vol. 31, no. 10, pp. 1182–1193, 2003.
[27] X. Y. Luo and T. J. Pedley, "A Numerical Simulation of Steady Flow in a 2-D Collapsible Channel," *Journal of Fluids and Structures*, vol. 9, no. 2, pp. 149–174, 1995.
[28] O. E. Jensen, "Instabilities of flow in a collapsed tube," *Journal of Fluid Mechanics*, vol. 220, pp. 623–659, 1990.